Original Article

BARX2/FOXA1/HK2 axis promotes lung adenocarcinoma progression and energy metabolism reprogramming

Kai Xie[1,2#], Jian Feng[2,3#], Dingwei Fan[2#], Shi Wang[2], Jing Luo[4], Zhijian Ren[2], Chao Zheng[5], Yifei Diao[4], Ramon Andrade De Mello[6,7,8], Simona Tavolari[9,10], Giovanni Brandi[11], Anja C. Roden[12], Binhui Ren[2], Yi Shen[1,4,5], Lin Xu[2]

[1]Department of Cardiothoracic Surgery, Jinling Hospital, School of Nanjing Medical University, Nanjing, China; [2]Department of Thoracic Surgery, The Affiliated Cancer Hospital of Nanjing Medical University & Jiangsu Cancer Hospital & Jiangsu Institute of Cancer Research, Jiangsu Key Laboratory of Molecular and Translational Cancer Research, Nanjing, China; [3]Department of Thoracic Surgery, Shanghai Chest Hospital, Shanghai Jiao Tong University, Shanghai, China; [4]Department of Cardiothoracic Surgery, Jinling Hospital, Medical School of Nanjing University, Nanjing, China; [5]Department of Cardiothoracic Surgery, Jinling Hospital, School of Medicine, Southeast University, Nanjing, China; [6]Division of Medical Oncology, Hospital 9 de Julho, São Paulo, SP, Brazil; [7]Post-Graduation Programme in Medicine, School of Medicine, Nove de Julho University (UNINOVE), São Paulo, SP, Brazil; [8]Algarve Biomedical Centre, Department of Biomedical Sciences and Medicine, University of Algarve, Faro, Portugal; [9]Department of Experimental Diagnostic and Specialty Medicine, S. Orsola-Malpighi University Hospital, Bologna, Italy; [10]Center for Applied Biomedical Research, S. Orsola-Malpighi University Hospital, Bologna, Italy; [11]Department of Experimental, Diagnostic and Speciality Medicine, 'L. & A. Seragnoli' Institute of Hematology and Medical Oncology, Sant'Orsola-Malpighi Hospital, Bologna, Italy; [12]Department of Laboratory Medicine and Pathology, Mayo Clinic, Rochester, MN, USA

Contributions: (I) Conception and design: K Xie, Y Shen, B Ren; (II) Administrative support: L Xu, B Ren; (III) Provision of study materials or patients: J Feng, D Fan, S Wang; (IV) Collection and assembly of data: J Luo, Z Ren; (V) Data analysis and interpretation: C Zheng, Y Diao; (VI) Manuscript writing: All authors; (VII) Final approval of manuscript: All authors.

[#]These authors contributed equally to this work.

Correspondence to: Binhui Ren, MD. Department of Thoracic Surgery, The Affiliated Cancer Hospital of Nanjing Medical University & Jiangsu Cancer Hospital & Jiangsu Institute of Cancer Research, Jiangsu Key Laboratory of Molecular and Translational Cancer Research, 42 Baiziting Road, Nanjing, China. Email: renbinhui@jszlyy.com.cn; Yi Shen, MD. Department of Cardiothoracic Surgery, Jinling Hospital, Medical School of Nanjing University, 305 East Zhongshan Road, Nanjing, China. Email: dryishen@nju.edu.cn; Lin Xu, MD. Department of Thoracic Surgery, The Affiliated Cancer Hospital of Nanjing Medical University & Jiangsu Cancer Hospital & Jiangsu Institute of Cancer Research, Jiangsu Key Laboratory of Molecular and Translational Cancer Research, 42 Baiziting Road, Nanjing, China. Email: xulin83@njmu.edu.cn.

Background: Metabolic reprogramming is an emerging cancer feature that has recently drawn special attention since it promotes tumor cell growth and proliferation. However, the mechanism of the Warburg effect is still largely unknown. This research aimed to reveal the effects of BarH-like homeobox 2 (*BARX2*) in regulating tumor progression and glucose metabolism in lung adenocarcinoma (LUAD).

Methods: Expression of *BARX2* was measured by quantitative real-time polymerase chain reaction (qRT-PCR) in LUAD cell line and tissues, and the tumor-promoting function of *BARX2* in LUAD cells was detected *in vitro* and *in vivo* xenograft models. The metabolic effects of *BARX2* were examined by detecting glucose uptake, the production levels of lactate and pyruvate, and the extracellular acidification rate (ECAR). Chromatin immunoprecipitation (ChIP) assay and luciferase reporter gene assay were used to identify the underlying molecular mechanism of *BARX2* regulation of *HK2*. Further studies showed that transcription factor *FOXA1* directly interacts with *BARX2* and promotes the transcriptional activity of *BARX2*.

Results: *BARX2* was remarkably up-regulated in LUAD tissues and positively linked to advanced clinical stage and poor prognosis. *In vitro* and *in vivo* data indicated ectopic expression of *BARX2* enhanced cell proliferation and tumorigenesis, whereas *BARX2* knockdown suppressed these effects. Metabolic-related experiments showed *BARX2* promoted the reprogramming of glucose metabolism. Mechanistically, the *BARX2/FOXA1/HK2* axis promoted LUAD progression and energy metabolism reprogramming.

Conclusions: In summary, our research first defined *BARX2* as a tumor-promoting factor in LUAD and

that it may act as a novel prognostic biomarker and new therapeutic target for the disease.

Keywords: Transcription factor; *BARX2*; lung adenocarcinoma (LUAD); glucose metabolism; *HK2*

Submitted Mar 22, 2022. Accepted for publication Jul 15, 2022.
doi: 10.21037/tlcr-22-465
View this article at: https://dx.doi.org/10.21037/tlcr-22-465

Introduction

Lung cancer is the most common fatal cancer worldwide, with over 2.2 million new cases and 1.78 million deaths annually (1). Non-small-cell cancer (NSCLC), including lung adenocarcinoma (LUAD) and lung squamous cell carcinomas (LUSC), accounts for 80–85% of all cases (2). Despite advances in cancer treatment, LUAD patients' prognosis is far from satisfying (3). Although treatment of LUAD has met with significant progress in recent times, the overall survival (OS) of LUAD patients remains suboptimal, and valuable molecular biomarkers are lacking. Consequently, investigating the underlying pathogenesis of LUAD is of significant importance in improving its early diagnosis and effective treatment.

Cancer cells are often subjected to various environmental stresses such as nutritional deficiencies, hypoxia, and acidosis (4), and to fulfil energy and biosynthetic needs, they metabolize substrates such as glucose and fatty acids through metabolic reprogramming (5). The aberrant metabolic characteristic of tumors is considered a hallmark of cancer, and cancer cells preferentially utilize the glycolytic pathway to produce more pyruvate and lactate even when sufficient oxygen is available, leading to acidification of the microenvironment (5,6). This phenomenon is also termed Warburg effect, in which cancer cells grow through differential uptake of glucose and amino acids, and increased biosynthesis of lipids, proteins, and nucleic acid (7). Warburg effect within the tumor microenvironment results in an accumulation of lactic acid, which acidifies the tumor microenvironment. In recent studies, it has been shown that tumor cells can escape immune surveillance due to an accumulation of lactic acid (8,9). An increasing number of studies have aimed to explore the actual link between metabolic processes and oncogenesis (10), and pharmacological agents targeting critical regulators of glucose metabolism are in development (11,12). It is well known that transcription factors are critical in regulating the Warburg effect (13), including *p53*, *MYC*, and *HIF-1α* which are responsible for the metabolic switch from oxidative phosphorylation to the glycolysis pathway in tumor cells.

Homeodomain transcription factors participate in tumorigenesis and developmental processes by controlling cellular behaviour such as proliferation, adhesion, migration, differentiation, and apoptosis (14,15). The BarH-like homeobox 2 (*BARX2*) gene is a homeodomain factor in the Bar family located in this critical LOH region 11q24-q25 region (16,17), and is a crucial regulator of cell adhesion, cytoskeleton remodeling, and growth factor signaling (18-21). *BARX2*-deficient mouse embryos show defective heteromorphic regeneration (22). Furthermore, *BARX2* plays a pivotal role in many cancers, particularly urinary bladder cancer (23) and gastric cancer (24). Although *BARX2* is a transcription factor, its role in regulating tumor metabolism remains unclear. HK2 is the rate-limiting enzyme catalyzes the first irreversible step of glycolysis (25). The increasing evidence indicates that HK2 overexpression and poor prognosis are strongly associated in multiple human cancers (26-28). Forkhead box A1 (*FOXA1*) is a member of a group of transcription factors known as pioneer factors. *FOXA1* binds to condensed chromatin and allows subsequent binding of other transcription factors (29). Several studies have shown that *FOXA1* plays roles oncogenic in NSCLC cells (30,31).

In this study, we aimed to determine metabolism-related transcription factors and discover their underlying mechanisms. Our analyses demonstrated that *BARX2* is frequently upregulated in LUAD, and its upregulation is linked to poorer patient survival. *In vitro* and *in vivo* functional experiments indicated *BARX2* may regulate cell proliferation and tumorigenicity. Mechanistically, our findings suggest that the *BARX2/FOXA1/HK2* axis promotes LUAD progression and energy metabolism reprogramming. We present the following article in accordance with the ARRIVE reporting checklist (available at https://tlcr.amegroups.com/article/view/10.21037/tlcr-22-465/rc)

Methods

Clinical specimens

LUAD and corresponding adjacent normal lung tissues were harvested from 2017–2021 at the Department of Thoracic Surgery, Jiangsu Cancer Hospital. The samples were snap-frozen in liquid nitrogen immediately after resection. The study was conducted in accordance with the Declaration of Helsinki (as revised in 2013). The study was approved by ethics board of Jiangsu Cancer Hospital. Informed consent was taken from all the patients.

Cell culture

All cell lines [PC9, A549, NCI-1975, NCI-H1299, and human bronchial epithelial cell (HBE)] were purchased from the Shanghai Institute for Biological Science, China. PC9, A549, NCI-1975, and NCI-H1299 cells were cultivated in DMEM (KeyGene, Nanjing, China) with high glucose (4.5 g/L) and 10% fetal bovine serum, and HBE cells were cultivated in RPMI 1640 (KeyGene, Nanjing, China), supplemented with 10% fetal bovine serum. All cell lines were maintained in a humidified incubator at 37 ℃ (5% CO_2).

Tissue microarrays (TMAs) and immunohistochemistry (IHC)

LUAD TMAs, obtained from Shanghai Outdo Biotech Co. Ltd. (Cat. No. HLugA180Su04) was analyzed for *BARX2* expression. The pathologic stage was determined according to the Union for International Cancer Control (UICC) TNM staging system (8th edition). The sections were incubated with an anti-BARX2 antibody (Clone ARG-10900; arigo Biolaboratories, Shanghai, China; 1:1,000) and the IHC scores were calculated according to intensity and percentage of positive cells. The staining intensity was scored as following: 0 (negative), 1 (weak), 2 (moderate), or 3 (strong). The H score (percentage of positive cells multiplied by respective intensity scores) was used as the final staining score (a minimum value of 0 and a maximum value of 300).

IHC assays were performed as standard protocols. In brief, mouse tissue sections were deparaffinized in xylene and rehydrated in graded alcohol (100%, 96%, 70%). Endogenous peroxidase activity was blocked by 3% hydrogen peroxide incubation and antigen extraction, while the antibody used for immunostaining was the anti-*BARX2* antibody.

RNA extraction and quantitative RT-PCR

Total RNA was isolated using Trizol reagent (Invitrogen) from cells or tissue samples according to the manufacturer's guidelines. Relative RNA level was measured using the SYBR Select Master Mix (Applied Biosystems, Cat: 4472908. KeyGEN, Nanjing, China) by quantitative real-time polymerase chain reaction (qRT-PCR), using GAPDH as endogenous control. The relative amount levels of RNA were calculated using the comparative $2^{-\Delta\Delta CT}$ method. All primer sequences are listed in Table S1.

Western blotting

Western blot assays were performed according to the manufacturer's protocol (32). Anti-β-actin antibody (Clone 3700; Cell Signaling Technology, Danvers, Massachusetts, USA; 1:1,000) was used as a loading control. The antibodies were purchased from the following manufacturers: anti-*BARX2* (Clone ARG-10900; arigo Biolaboratories, Shanghai, China; 1:1,000), anti-*FOXA1* (Clone 53528S; Cell Signaling Technology, Danvers, Massachusetts, USA; 1:1,000), anti-*HK2* (Clone 2867T; Cell Signaling Technology, Danvers, Massachusetts, USA; 1:1,000).

Plasmid vectors and siRNAs transfection

Plasmid vectors or siRNAs were transfected with Lipofectamine™ 3000 Transfection Reagent (Invitrogen, CA, USA) or Lipofectamine RNAiMAX (Invitrogen, CA, USA), respectively, according to the manufacturer's guidelines. The specific siRNA and transfection plasmid vectors were purchased from RiboBio. All siRNA sequences are shown in Table S2.

Cell proliferation and migration/invasion assays

After 24 hours (h) of transfection, cells were harvested for assessment of cell proliferation, which was then examined by a cell counting kit-8 (CCK-8). Cells were plated overnight in 96-well plates at a controlled density of 2,000 cells per well, then CCK-8 (10 μL/well) was added to each well before incubation for 2 h. The reaction products were measured at 450 nm according to the manufacturer's instructions. xCELLigence analysis system (RTCA) was performed to monitor real-time cell proliferation, and 8,000 cells per well were added on E-plates 16, with the proliferation curve tested every half hour for cell index up

to 90 h. For the EdU incorporation experiment, the Cell-Light™ EdU Apollo®488 In Vitro Imaging Kit (RiboBio, Guangzhou, China) was used and the assay was performed according to the instructions. To calculate the number of cells: Open ImageJ software, choose File->Open (select the image to Analyze), and Plugins->Analyze->CellCounter. First click Initialize, and then select the cell types to be counted respectively. Define the blue one as Type 1 and the green one as Type 2. Select Type 1 and click the blue dot in the picture one by one, and the total number of cells will be displayed in the box after Type 1. For migration/invasion assays, 5×10^4 cells were seeded on Transwell kits (8 mm PET, 24-well Millicell) or Matrigel-coated inserts (BD Biosciences, Bedford, MA, USA). After 24 or 48 h of incubation, cells were fixed with methanol and stained with 0.1% crystal violet, imaged, then counted under the microscope. To calculate the number of cells: Open ImageJ software, go to Type ->8-bit to change the Image from RGB to 8-bit, then go to Edit -> Invert, then Image -> Adjust -> Threshold... To open the threshold window and set the threshold. Adjust the Threshold through the Threshold window Threshold, and the cells whose brightness exceeds the Threshold will be counted. After setting, click the Apply button to Apply it to the picture. If two, three or more cells are found to overlap, you can separate the cells using the Watershed method by going to Process -> Binary -> Watershed. Then click Analyze -> Analyze Particles..., set the nucleus size, select display outline or other options. Click OK to analyze these points of interest. Three Windows will pop up, namely Summary, Results and ROI Manager, summarizing the total number of these points (nucleus) and various parameters of each point (such as area, average value, width, height, etc.). Each point can be manipulated (add or delete, etc.) through ROI Manager. Finally, you can see the total number of cells in the image in the Summary Windows. Each experiment was determined in triplicate, independently.

Metabolic assays

A Glucose Uptake Assay Kit (Abcam, Cambridge, UK), L-lactate Assay Kit (Abcam, Cambridge, UK), Pyruvate Assay Kit (Abcam, Cambridge, UK), and Seahorse XF Glycolysis Stress Test kit (Agilent, Beijing, China) were used for detecting glucose, lactate, pyruvate, and ECAR, respectively, and performed according to the standard protocols. Cells were seeded in 6-well plates and cultured overnight, before the supernatant was collected, and glucose, lactate, and pyruvate were measured. For ECAR detection, cells were seeded in XF 24-well plates with 1×10^4 cells and starved overnight. ECAR was monitored by the Seahorse XF 24 Extracellular Flux Analyzer (Agilent, Beijing, China). The results were normalized to the protein content, and each experiment was determined in triplicate independently.

Chromatin immunoprecipitation (ChIP)

ChIP assays were performed by ChIP Assay Kit (Sigma-Aldrich) according to the manufacturer's protocol (32). We used 5 μg anti-*BARX2* antibody or 5 μg anti-*FOXA1* antibody for each reaction, and 5 μg mouse IgG (Abcam; Cat: ab-150115) was applied as the control. The purified ChIP DNA samples were subjected to PCR amplification. All specific primer sequences are listed in Tables S3. GAPDH was used as control.

Luciferase reporter assay

Luciferase reporter assays were assessed by the Dual-Luciferase Reporter Assay System (Promega, Madison, WI, USA). The 3'UTR of *FOXA1* or *BARX2* containing the predicted binding site for *BARX2* or *HK2* was cloned into a pGL4-basic luciferase reporter vector. CMV-Renilla was applied as control. The luciferase activity was measured by Firefly/Renilla value. Transfection was performed using Lipofectamine™ 3000 Transfection Reagent (Invitrogen, CA, USA) according to the manufacturer's recommendations.

Xenograft model

To avoid possible effects of sex on mice survival, tumor growth, and tumor implantation response, mice of the same sex were used. In comparison to male mice, female mice are more docile and easier to work with. Twelve female nude BALB/c mice purchased from Nanjing Medical University at 4–6 weeks and in good growth condition were randomly divided into two groups. PC9 cells were cultured in large dishes until logarithmic growth phase and transfected when the density reached 70–80% with *BARX2* interference plasmid (sh-*BARX2*) and control plasmid (sh-NC) respectively. Cells were then counted 48 h after transfection following trypsin digestion, washed with phosphate buffered saline (PBS), and resuspended in serum-free medium. We then selected 1×10^7 cells and suspended them in PBS to construct a

subcutaneous lotus tumor model. Mice were housed in 485×350×200 mm cages and were fed with a full-price pellet diet under conditions of free water, room temperature 22±2 ℃, humidity 50–60%, and a well ventilated 12:12 h light/dark cycle. Tumor longitudinal and transverse diameters were measured weekly, and tumor volume (TV) was calculated by the formula: TV =1/2 × longer diameter × shorter diameter^2. The health of the animals was monitored twice a day during the feeding period, and no adverse events were observed. At the start of the experiments animals weighed [mean ± standard deviation (SD)] 17.8±0.3 grams. Nude mice were sacrificed 6 weeks after cell injection, the tumor was excised, weighed, and retained for subsequent experiments. Experimenters were blinded to the pharmacological treatment while processing data and making exclusion decisions. Animal experiments were approved by the ethics board of Nanjing Medical University (No. 2018-122), in compliance with Chinese guidelines for the care and use of animals. The mean value was expressed as mean ± SD, the inter-group analysis was statistically processed by *t*-test, and the results were statistically analyzed by SPSS (Statistical Package for the Social Science) 22.0.

Statistical analysis

All statistical data analyses were performed with SPSS 22.0 and the data visualization using GraphPad Prism for Windows v.8.0. The results are presented throughout as mean values ± SD from the three experiments independently. The Student *t*-test identified the continuous variable between the two groups or more than two groups, and P value <0.05 was considered statistically significant difference.

Results

BARX2 is highly expressed in LUAD tissues and correlates with poorer prognosis

To evaluate the role of *BARX2* in LUAD, we first compared its mRNA expression between 60 LUAD and corresponding non-tumor tissues by qRT-PCR. These studies revealed that BARX2 expression was remarkably higher in 97% (57/60) of LUAD tissues (*Figure 1A*). We then assessed whether *BARX2* expression was up-regulated in LUAD cells compared with HBE by Western blot and qRT-PCR (*Figure 1B,1C*). The The Cancer Genome Atlas (TCGA) dataset indicated that *BARX2* expression was significantly higher in LUAD samples than in non-neoplastic lung samples (P<0.001) (*Figure 1D*). Similarly, *BARX2* was also markedly higher expressed in 57 LUAD samples than matched non-neoplastic lung samples (P<0.001) (*Figure 1E*). The receiver operating characteristic (ROC) curves indicated that *BARX2* could distinguish LUAD tissue from normal lung tissue with confidence interval (CI) =0.839–0.905 (area under the ROC curve, 0.872) (*Figure 1F*). Furthermore, the high or low *BARX2* expression of LUAD from the TCGA database was defined as a value in the top quartile or bottom quartile of the set, respectively. The overall survival (OS) analysis of patients indicated that high *BARX2* expression was associated with poor OS (P=0.043) (*Figure 1G*).

IHC assays were performed on TMAs to detect the protein expression of *BARX2* in 92 human LUAD tissues and 88 adjacent non-neoplastic lung tissues. IHC images of one patient were presented (*Figure 1H*), and results showed that staining scores of *BARX2* were higher in cancer tissues (P<0.001, *Figure 1I*). Combined with the patients' clinical information, the expression of *BARX2* was higher in patients with more advanced TNM stage (stage I–II *vs.* III–IV, P<0.001, *Figure 1J*), T stage (T1-2 *vs.* T3–T4, P<0.001, *Figure 1K*), N stage (N0 *vs.* N1, P<0.001, *Figure 1L*), and lymph node metastasis (P<0.001, *Figure 1M*). By ranking the expression of *BARX2* in 92 tissues from high to low, we defined the 'high *BARX2* expression' group (n=46) and the 'low *BARX2* expression' group (n=46) according to the median level of *BARX2* to explore the prognostic significance of *BARX2* in LUAD. Survival analysis showed patients with high *BARX2* expression had a more dismal OS than patients with low *BARX2* expression (P<0.001, *Figure 1N*).

Together, these data demonstrated *BARX2* was highly expressed in LUAD tissues in comparison to adjacent non-neoplastic lung tissue and was associated with poor outcomes.

Knockdown of BARX2 inhibited LUAD cell proliferation and progression in vitro and in vivo

To explore the biological function of *BARX2* in LUAD cells, *BARX2* was knocked down by transfecting siRNAs-*BARX2* into PC9 cells; the successful transfection was verified by qRT-PCR and Western blot (*Figure 2A,2B*). The results of CCK8 (*Figure 2C*), RTCA (*Figure 2D*), and EdU staining assays (*Figure 2E,2F*) showed that silencing of *BARX2* significantly suppressed the proliferation of PC9 cells. In addition, Transwell and Matrigel assays were utilized, measuring the greatly inhibited migration and invasion abilities in siRNAs-*BARX2* groups (*Figure 2G,2H*). Moreover, we transfected plasmids overexpressing *BARX2*

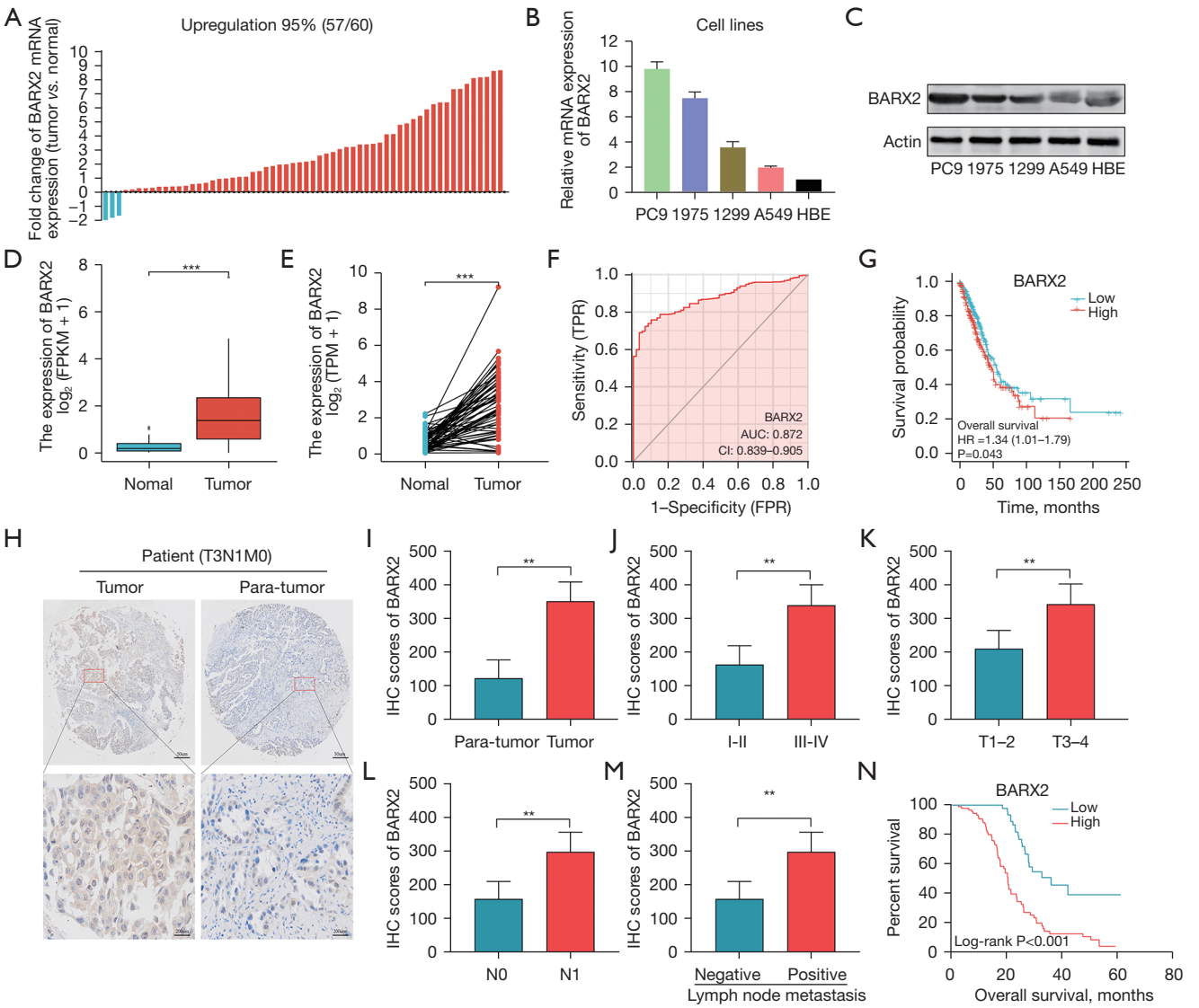

Figure 1 *BARX2* is upregulated in LUAD tissues and positively correlates with aggressive clinical characteristics. (A) *BARX2* expression in LUAD tissues determined by RT-PCR. (B,C) The expression of *BARX2* in LUAD cell lines is higher than HBE. (B) qRT-PCR. (C) Western blot. (D,E) The mRNA expression of *BARX2* (D) in normal tissues and tumor tissues and (E) in paired tissues. (F) A ROC curve to test the value of *BARX2* and to identify LUAD tissues. (G) Kaplan-Meier curve for OS in LUAD based on *BARX2* expression levels. (H) Representative IHC staining images in TMAs were shown. (I) The *BARX2* staining score was up-regulated in LUAD compared with that in adjacent normal tissues (P<0.001). (J-M) The *BARX2* staining score was positively correlated with (J) TNM stage (P<0.001), (K) T stage (P<0.001), (L) N stage (P<0.001), and (M) lymph node metastasis (P<0.001) LUAD patients. (N) Patients with high expression of BARX2 have poor OS in LUAD (P<0.001). **, P<0.01; ***, P<0.001. HBE, human bronchial epithelial cell; LUAD, lung adenocarcinoma; qRT-PCR, quantitative real-time polymerase chain reaction; FPKM, fragment per kilo base per million mapped reads; TPM, transcripts per million; ROC, receiver operating characteristic curve; TPR, true positive rate; FPR, false positive rate; CI, confidence interval; AUC, area under ROC curve; OS, overall survival; IHC, immunohistochemistry; TMAs, tissue microarrays.

into A549 cells. The results showed that overexpression promoted the proliferation, migration, and invasion of A549 cells (Figure S1A-S1E).

To investigate the tumorigenic effects of *BARX2 in vivo* using xenograft tumor models, PC9 cells transfected with NC-shRNA or *BARX2*-shRNA were injected into nude

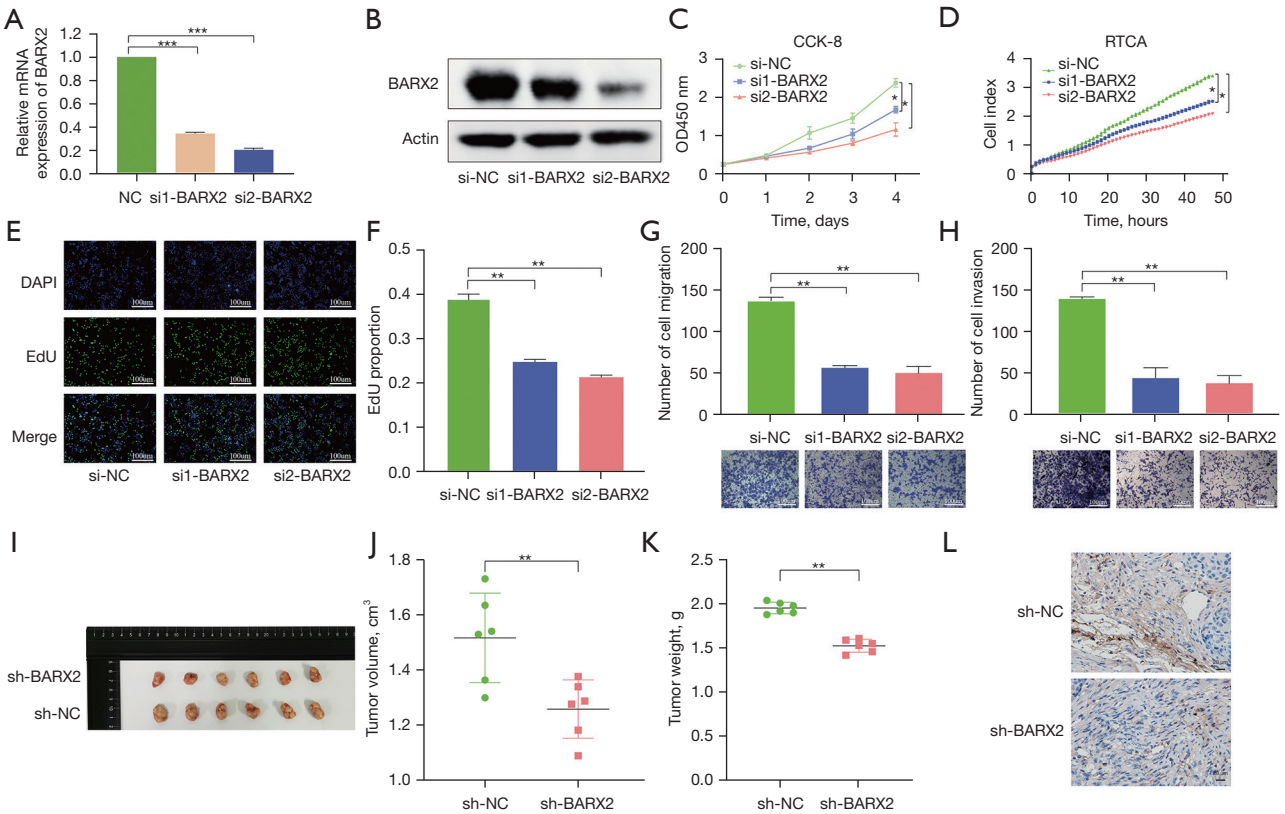

Figure 2 Knockdown of *BARX2* inhibited proliferation and progression *in vitro* and *in vivo*. (A,B) Two specific siRNA (si1 and si2) of *BARX2* were designed and synthesized, and the transfection efficiency in PC9 cells was measured by (A) qRT-PCR and (B) Western blotting. (C-F) CCK-8 (C), RTCA (D), and EdU (E,F) staining assays indicated knockdown of *BARX2* inhibited growth of PC9 cell lines, respectively. (G,H) Transwell (G) and Matrigel (H) assays were used to test the migration and invasion ability of PC9 cells after knockdown expression of *BARX2*, respectively. After migration/invasion, the remaining cells on the top filter were washed off, and the filters were fixed in 4% methanol for 30 minutes. Filters were washed again in PBS before staining in 0.1% crystal violet for 30 min and then counted under the microscope. (I) Images of xenograft tumors derived from nude mice bearing PC9 cells of different groups. (J) Tumor volume was measured every week after injection. (K) Tumor weight was measured after resection of xenograft tumors. (L) Immunohistochemistry of tumor nodules by specific antibody were shown. *, P<0.05; **, P<0.01; ***, P<0.001. qRT-PCR, quantitative real-time polymerase chain reaction; OD, optical density; RTCA, real time cellular analysis; CCK8, cell counting kit-8; PBS, phosphate buffer saline.

mice. The results indicated that *BARX2*-deficient PC9 cells dramatically inhibited tumor growth (volume and weight) (*Figure 2I-2K*). IHC analysis revealed that tumors derived from sh-*BARX2* transfected cells showed less staining of BARX2 than those in the sh-NC group (*Figure 2L*).

BARX2 contributed to the Warburg effect in LUAD cells

We performed GSEA using the low-*BARX2* and high-*BARX2* expression datasets to identify the potential function of *BARX2* in LUAD, and multiple GSEA showing glycose metabolism-related pathways (Table S4). It is well known that metabolic reprogramming plays a pivotal role in tumorigenesis and is commonly observed in multiple cancers (7,33,34). Metabolic reprogramming is considered an emerging hallmark of cancer (4,35). Tumor cells provide adenosine triphosphate (ATP) for growth mainly through glycolysis and biomolecules for cell replication through the pentose phosphate pathway (36,37). Moreover, even under adequate oxygen conditions, tumor cells preferentially use glycolysis to produce high levels of secreted lactate, which is known as the Warburg effect (*Figure 3A*). Consequently, we hypothesized that *BARX2* might be a key factor for metabolic reprogramming in LUAD cells. As expected, the

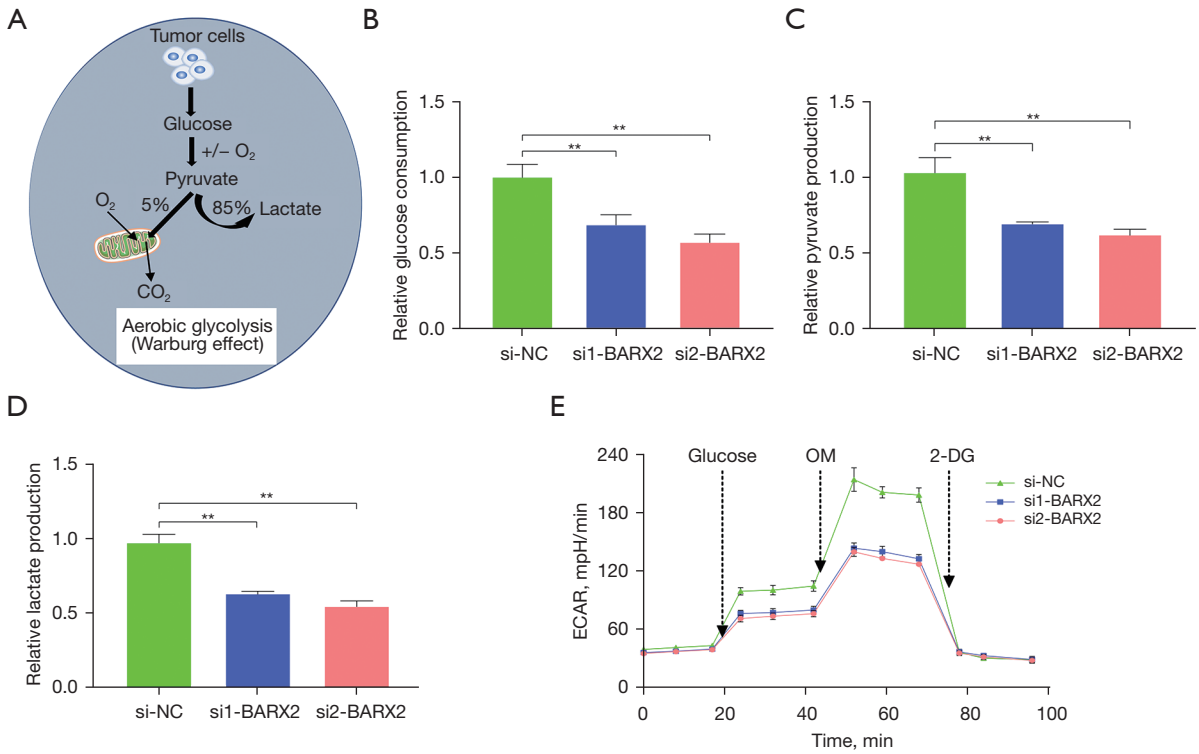

Figure 3 *BARX2* contributed to the Warburg effect in LUAD cells. (A) Schematic depicting the Warburg effect in cancer cells. (B-D) Detection of (B) glucose consumption, (C) pyruvate, and (D) lactate production in PC9 cells after knockdown expression of *BARX2*. (E) ECAR were measured by Seahorse XF in PC9 cells after knockdown expression of *BARX2*. **, P<0.01. qRT-PCR, quantitative real-time polymerase chain reaction; OM, oligomycin; 2-DG, 2-deoxy-glucose; LUAD, lung adenocarcinoma; ECAR, extracellular acidification rate.

results showed *BARX2* knockdown leads to a reduction in glucose consumption, and lactate and pyruvate production (*Figure 3B-3D*). Next, we explored whether *BARX2* could directly affect the metabolism of LUAD cells by assaying the rate of ECAR (38). Seahorse analysis revealed that ECAR was reduced in PC9 cells by inhibiting the expression of *BARX2* (*Figure 3E*). In addition, overexpression of *BARX2* significantly promoted glucose consumption and increased the production of lactate, pyruvate, and ECAR in A549 cells (Figure S2A-S2D). The above results implied that *BARX2* contributed to the Warburg effect in LUAD cells.

BARX2 exerts a cancer-promoting effect by regulating HK2

Reprogramming of glucose metabolism in tumors drives the transition to aerobic glycolysis and lactate production by regulating the expression and activation of glycolytic enzymes, including *HK2* (hexokinase 2), glucose transporter 1/4 (*GLUT1/4*, *SLC2A1/4*), *GPI* (glucose-6-phosphate isomerase), *PFKL* (6-phosphofructokinase, liver type), *ALDO* (aldolase A), *GAPDH* (glyceraldehyde 3-phosphate dehydrogenase), *ENO* (enolase 1), *PKM2* (pyruvate kinase M2), and *LDHA* (lactate dehydrogenase A) (39) (*Figure 4A*). To explore whether *BARX2* could affect these metabolism-related enzymes, we used qRT-PCR. The results demonstrated the mRNA and protein level of *HK2* was dramatically downregulated by BARX2 siRNA transfection (*Figure 4B,4C*). *HK2* is a cancer-related isoenzyme that catalyzes the first rate-limiting step of glucose metabolism and is a crucial key link in integrating energy production, protecting mitochondrial integrity and cell survival (40). To confirm whether *BARX2* functions via expression of *HK2*, the plasmid overexpress *HK2* was transfected into PC9 cells and treated with si-*BARX2* for rescue experiments. The results showed that overexpression of *HK2* could reverse the ability of cell proliferation, migration, and invasion compared to the si-*BARX2* group (*Figure 4D-4F*). Similar findings were noted for the metabolic phenotype, including glucose consumption, lactate, pyruvate, and ECAR production (*Figure 4G-4J*). These results indicated that

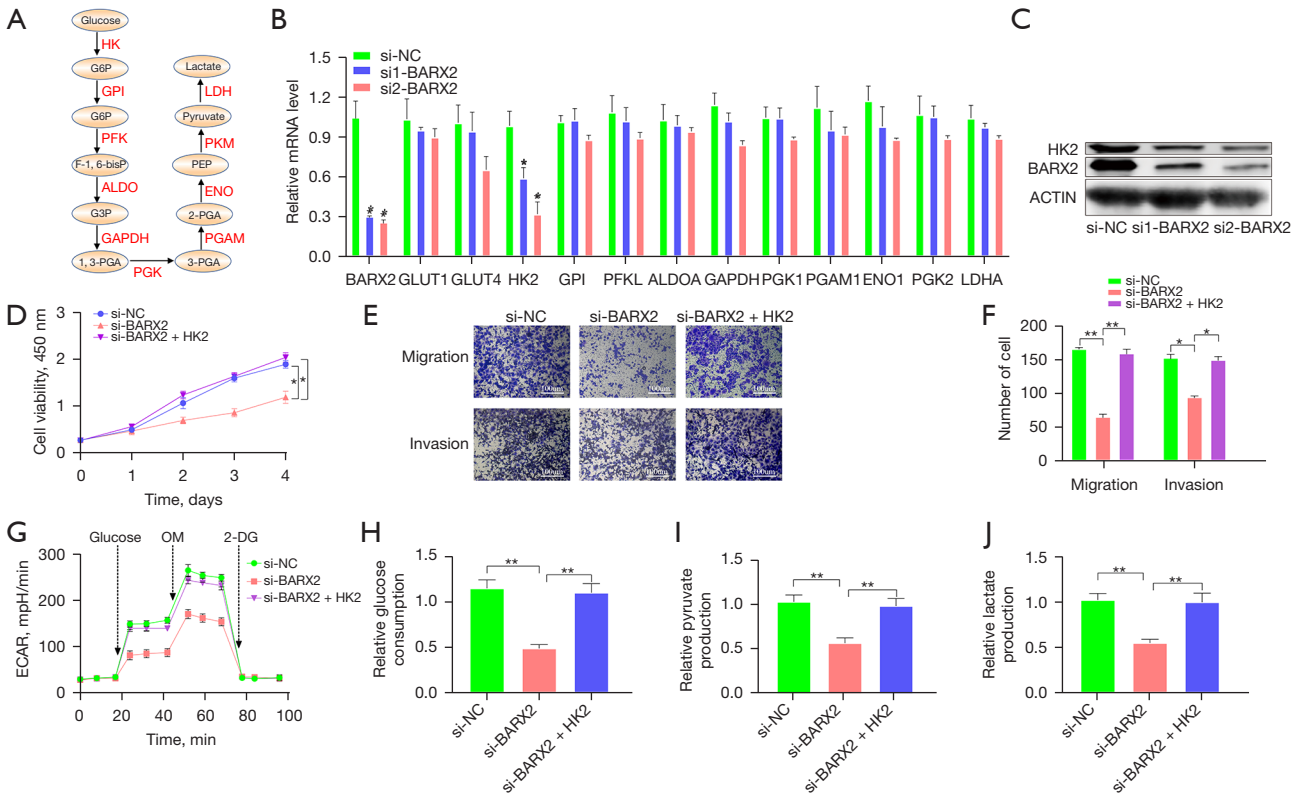

Figure 4 *BARX2* exerts cancer-promoting effect by regulating *HK2*. (A) Diagram of key enzymes that play key roles in glucose metabolism reprogramming. (B) The mRNA expression of metabolism-related genes was measured by qRT-PCR after knockdown expression of *BARX2* in PC9 cells. (C) The protein expression of *HK2* was measured by Western blotting after knockdown expression of *BARX2* in PC9 cells. (D) Overexpression of *HK2* restored the inhibition effect of *BARX2* on proliferation in PC9 cells. (E,F) Overexpression of *HK2* restored the inhibition effect of *BARX2* on migration (E) and invasion (F) in PC9 cells. After migration/invasion, the remaining cells on the top filter were washed off, and the filters were fixed in 4% methanol for 30 minutes. Filters were washed again in PBS before staining in 0.1% crystal violet for 30 min and then counted under the microscope. (G-J) Overexpression of *HK2* restored the inhibition effect of *BARX2* on ECAR (G), glucose consumption (H), pyruvate production (I), and lactate production (J) in PC9 cells. *, P<0.05; **, P<0.01. qRT-PCR, quantitative real-time polymerase chain reaction; OM, oligomycin; 2-DG, 2-deoxy-glucose; ECAR, extracellular acidification rate; PBS, phosphate buffered saline.

BARX2 promoted tumor progression and glucose metabolism reprogramming of LUAD cells via upregulating *HK2*.

HK2 is a transcriptional target of BARX2 in LUAD

Transcription factors generally induce or repress gene expression through binding to their promoters. Therefore, we hypothesized that *HK2* is a transcriptional target of *BARX2*. As predicted by the Jaspar Database (41), we found a series of putative *BARX2* binding sites in the HK2 promoter with a calculated score of 10.759–5.83968 (Figure S3A). To confirm the hypothesis, we performed ChIP assay in LUAD cells to determine whether *BARX2* could bind to the HK2 promoter. A series of three sets of primers were designed to correlate with certain sites in the *HK2* promoter region (*Figure 5A*). The results showed that a component of the -1693 bp -1704 bp (Site1) site of the *HK2* promoter was enriched in chromosomal DNA precipitated by *BARX2* in PC9 and A549 cells (*Figure 5B,5C*). To provide more related data, luciferase reporter assays were performed which showed the *HK2* promoter region was amplified and cloned to the pGL4-basic vector and the empty pGL4-basic vector as a negative control, respectively. A mutant *HK2*-Luc reporter was also generated (*Figure 5D*). These data were in agreement with the result of ChIP experiments, indicating *BARX2* markedly promotes the luciferase activity of *HK2* in both PC9 and A549 cells (*Figure 5E,5F*). These results implied that *BARX2* was bound to *HK2*.

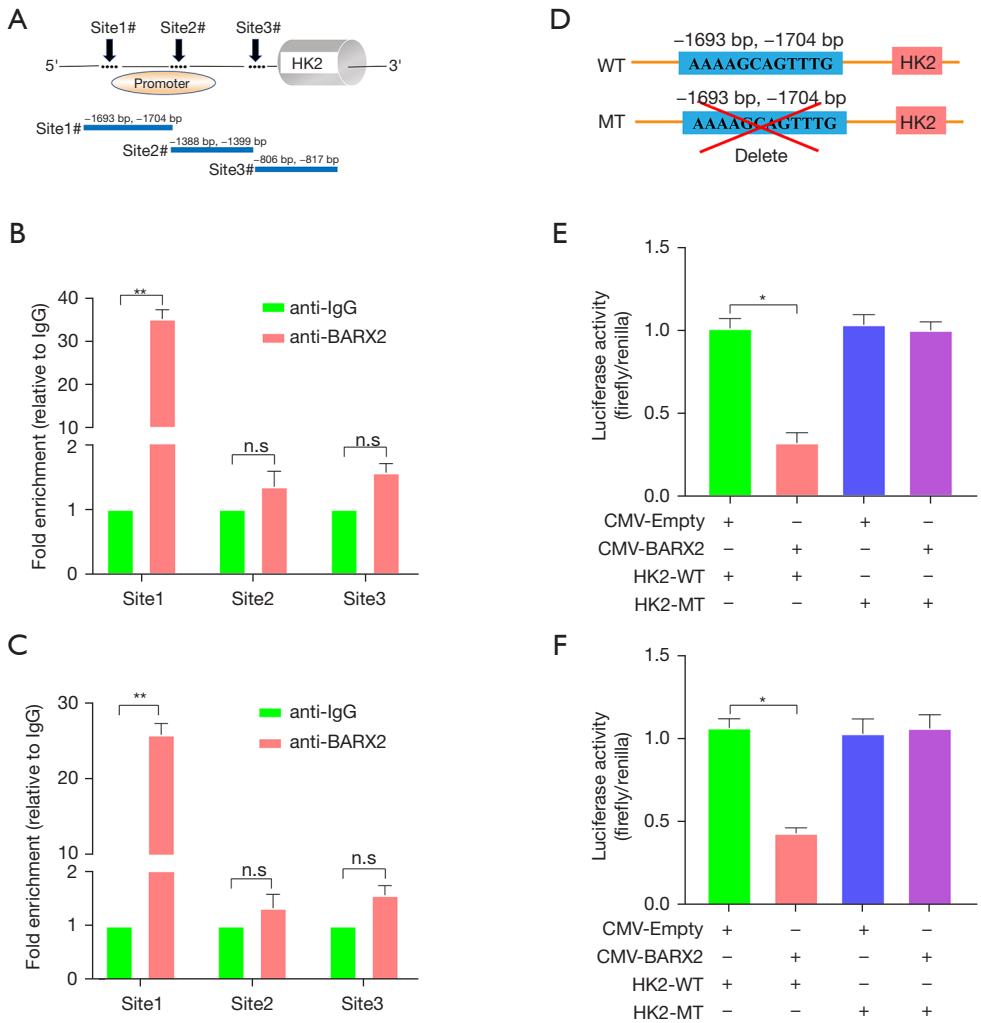

Figure 5 *HK2* was a transcriptional target of *BARX2* in LUAD. (A) Schematic of ChIP analysis in *HK2* promoter. (B,C) ChIP analysis demonstrated *BARX2* was directly bound to the region of the *HK2* promoter (sites #1) both in PC9 and A549 cells. (D) Schematic illustration of *BARX2* binding site on *HK2* promoter region and the mutant type were presented. (E,F) Luciferase assays demonstrated overexpression of *BARX2* remarkably decreased wild type but not mutant *HK2* promoter luciferase activity both in PC9 and A549 cells. *, P<0.05; **, P<0.01. n.s, not significant; LUAD, lung adenocarcinoma; ChIP, chromatin immunoprecipitation; WT, wild type; MT, mutant.

BARX2 is directly regulated by the transcription factor FOXA1

We sought to identify upstream transcriptional regulators that may lead to *BARX2* upregulation in LUAD using the UCSC Genome Browser and Jaspar Database. We predicted a series of transcription factors that bind to the *BARX2* promoter region. After screening, the transcription factor *FOXA1* attracted our interest as it can bind and open chromatin and trigger target transcription of target genes (42) and is also frequently amplified or mutated in human cancers (43,44). We verified that silencing *FOXA1* could down-regulate the expression of *BARX2* in PC9 cells (*Figure 6A,6B*). To understand whether *BARX2* was a direct target of *FOXA1*, we analyzed the *BARX2* promoter sequence using the JASPAR CORE database (Figure S3B). A series of three sets of primers were designed to correlate with certain sites in the *BARX2* promoter region (*Figure 6C*). ChIP assay revealed that *FOXA1* is mainly bound to the positions –515 to –529 bp (Site2) of the *BARX2* promoter (*Figure 6D*). Moreover, the result of the luciferase reporter was consistent with the ChIP assay and showed *FOXA1* could markedly promote the luciferase activity of *BARX2*

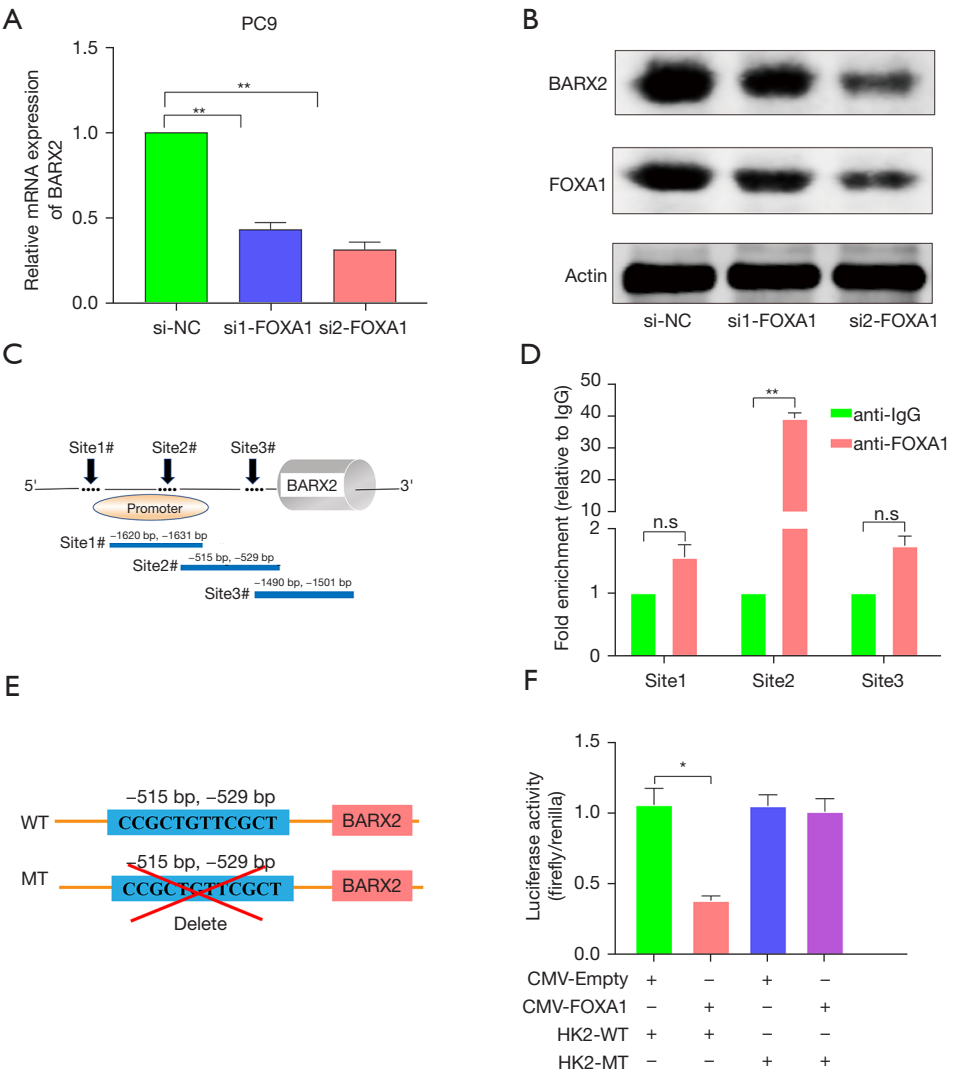

Figure 6 *BARX2* is directly regulated by the transcription factor FOXA1. (A,B) The expression of *BARX2* was measured by (A) qRT-PCR and (B) Western blotting after knockdown expression of FOXA1 in PC9 cells. (C) Schematic of ChIP analysis in *BARX2* promoter. (D) ChIP analysis demonstrated FOXA1 was directly bound to the region of the *BARX2* promoter (sites #2) in PC9 cells. (E,F) Overexpression of FOXA1 significantly reduced wild type but not mutant *BARX2* promoter luciferase activity in PC9 cells. *, P<0.05; **, P<0.01. n.s, not significant; qRT-PCR, quantitative real-time polymerase chain reaction; ChIP, chromatin immunoprecipitation; WT, wild type; MT, mutant.

markedly in PC9 cells (*Figure 6E,6F*). Taken together, our data revealed transcription factor FOXA1 as a critical regulator up-regulating *BARX2* at the transcriptional level in PC9 cells by directly binding to the *BARX2* promoter.

Discussion

Lung cancer is still a major health problem due to its high incidence and mortality rates. NSCLC accounts for 85% of all lung cancer (2). Even though extensive lung cancer studies have been conducted, the underlying pivotal molecular mechanism remains to be fully elucidated, hampering therapeutic strategies. As well known, solid tumors require high energy and nutrient supplies to support their rapid growth and reproduction processes. Moreover, glucose is the primary carbon source for cancer cells to fuel energy production and biosynthetic reactions (45). To survive, tumor cells must adapt to the

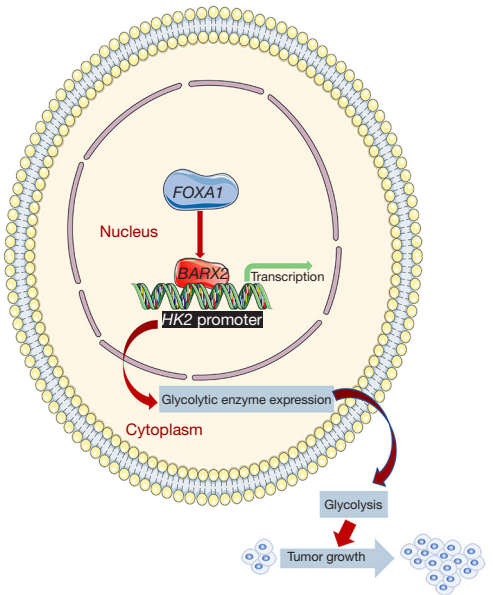

Figure 7 Schematic illustration of *BARX2/FOXA1/HK2* axis promotes LUAD progression and energy metabolism reprogramming. LUAD, lung adenocarcinoma.

harsh environments of nutrient stress and reduced pH and oxygen by increasing glucose uptake and lactate production; known as the Warburg effect (4). The increase in lactate production strongly supports diverse cancer cell activities, including cell proliferation, angiogenesis, and tumor invasion activity, promoting tumor aggressiveness (46,47). HIF-1 is a crucial element in the Warburg effect, which promotes disconnection of the TCA cycle from glycolysis and reductive glycolysis. A decrease in mitochondrial activity and an increase in membrane exchangers maintain an alkaline pH in the cell, which is favorable to glycolysis and cell cycle progression (48,49). Cancer stem cells that are inherently drug-resistant are often found in hypoxic niches and depend on glycolysis for survival (50). Although metabolic reprogramming has long been observed as a feature of neoplasia and tumor growth, the mechanism driving this process remains unclear. In this study, we attempted to target tumor therapy against LUAD from the point of glucose metabolism.

The transcription factor *BARX2* is a critical member of the Bar family of proteins and is expressed in some cancers. However, data regarding the role of *BARX2* in tumorigenesis has been somewhat conflicting (51,52). Interestingly, Chen *et al.* (53) showed the *BARX2* expression level was down-regulated in NSCLC. Therefore, *BARX2* has attracted our interest for further research.

In contrast to the study by Chen *et al.* (53) our results showed that *BARX2* was frequently up-regulated in LUAD tissues compared to non-neoplastic tissues. Furthermore, the TCGA database demonstrated that *BARX2* may be a potential predictive marker for LUAD tissues. In addition, clinical analysis revealed that upregulation of *BARX2* correlated with advanced tumor stage and poor prognosis of LUAD patients. Moreover, knockdown of *BARX2* significantly inhibited proliferation, invasion, migration, and glucose metabolism ability of LUAD cells *in vitro* and *in vivo*. These data imply that *BARX2* plays a vital role in promoting cancer progression, metastasis, and glucose metabolism of LUAD.

The GSEA results showed *BARX2* was related to glycose metabolism-related pathways. Tumor cells reprogram energy metabolism to facilitate cell growth and proliferation, a phenomenon which has been firmly established as a classical hallmark of cancer (4). The oncogenic metabolic reprogramming is driven by essential key enzymes including *HK2*, *GPI*, *PFKL*, *ALDO*, *GAPDH*, *ENO*, *PKM2*, and *LDHA* (54). Therefore, qRT-PCR and Western blotting were performed to validate the series of glycolytic enzymes. *HK2*, one protein remarkably decreased by *BARX2* knockdown, attracted our interest. *HK2* is a crucial enzyme that catalyzes the rate-limiting first step of glycolysis and is highly up-regulated in multiple human tumors (40). In addition, mechanistic investigations found that the expression of *BARX2* transcriptionally regulated *HK2*. We speculated that *BARX2* bound to the *HK2* promoter region promotes LUAD growth and metastasis.

While our study generated important and interesting findings, our results should be interpreted with caution. First, we found that the expression of *BARX2* was up-regulated in LUAD from TCGA database, then verified the up-regulation of *BARX2* expression in LUAD samples, LUAD tissue microarray, and LUAD cells, and verified that *BARX2* plays a carcinogenic role in LUAD through experiments *in vitro* and *vivo*. However, the results by Chen *et al.* (53) were different from ours. We speculated that there are several reasons: the LUAD samples we used come from different institutions and may be different; in addition, the cell lines we selected were different.

In summary, our findings first defined *BARX2* as a tumor promoter in LUAD and identified the *BARX2/FOXA1/HK2* axis as a pivotal pathway involved in its development and progression of LUAD (*Figure* 7). Targeting this axis could be a novel therapeutic strategy against LUAD.

Acknowledgments

The authors thank the Jiangsu Institute of Cancer Research and Jiangsu Key Laboratory of Molecular and Translational Cancer Research for providing technical platform support. The authors appreciate the academic support from the AME Thoracic Surgery Collaborative Group.

Funding: This research was supported by the National Natural Science Foundation of China (No. 82172642), National Natural Science Foundation for Youth of China (No. 81902354), National Natural Science Foundation for Youth of China (No. 81702444), and the Excellent Talents Fund Project of Xuzhou Medical University (No. XYFY2020017).

Footnote

Reporting Checklist: The authors have completed the ARRIVE reporting checklist. Available at https://tlcr.amegroups.com/article/view/10.21037/tlcr-22-465/rc

Data Sharing Statement: Available at https://tlcr.amegroups.com/article/view/10.21037/tlcr-22-465/dss

Conflicts of Interest: All authors have completed the ICMJE uniform disclosure form (available at https://tlcr.amegroups.com/article/view/10.21037/tlcr-22-465/coif). Prof. RAdM received research grant from CNPQ Brazil, Libss, Pfizer; royalties from Springer; consulting fee from Takeda; speaker fee from Merck, Pfizer, Novartis, Eurofarma, MSD, Bayer, Astrazenenca; supporting for attending meetings and stock from Merck. Prof. RAdM also serves in Advisory board for European School of Oncology and Brazilian Society of Cancerology. ACR received Royalties from educational material for thymic tumors; payment from Honorarium for grand rounds at NY Langone; and Travel support for visiting professorship at NYU Langone; none of them are pertinent to this publication. The other authors have no conflicts of interest to declare.

Ethical Statement: The authors are accountable for all aspects of the work in ensuring that questions related to the accuracy or integrity of any part of the work are appropriately investigated and resolved. The study was conducted in accordance with the Declaration of Helsinki (as revised in 2013). The study was approved by ethics board of Jiangsu Cancer Hospital. Informed consent was taken from all the patients. Animal experiments were approved by the ethics board of Nanjing Medical University (No. 2018-122), in compliance with Chinese guidelines for the care and use of animals.

References

1. Sung H, Ferlay J, Siegel RL, et al. Global Cancer Statistics 2020: GLOBOCAN Estimates of Incidence and Mortality Worldwide for 36 Cancers in 185 Countries. CA Cancer J Clin 2021;71:209-49.
2. Thai AA, Solomon BJ, Sequist LV, et al. Lung cancer. Lancet 2021;398:535-54.
3. Buddharaju LNR, Ganti AK. Immunotherapy in lung cancer: the chemotherapy conundrum. Chin Clin Oncol 2020;9:59.
4. Pavlova NN, Zhu J, Thompson CB. The hallmarks of cancer metabolism: Still emerging. Cell Metab 2022;34:355-77.
5. Intlekofer AM, Finley LWS. Metabolic signatures of cancer cells and stem cells. Nat Metab 2019;1:177-88.
6. Pavlova NN, Thompson CB. The Emerging Hallmarks of Cancer Metabolism. Cell Metab 2016;23:27-47.
7. Vaupel P, Schmidberger H, Mayer A. The Warburg effect: essential part of metabolic reprogramming and central contributor to cancer progression. Int J Radiat Biol 2019;95:912-9.
8. Romero-Garcia S, Moreno-Altamirano MM, Prado-Garcia H, et al. Lactate Contribution to the Tumor Microenvironment: Mechanisms, Effects on Immune Cells and Therapeutic Relevance. Front Immunol 2016;7:52.
9. Choi SY, Collins CC, Gout PW, et al. Cancer-generated lactic acid: a regulatory, immunosuppressive metabolite? J Pathol 2013;230:350-5.
10. Thakur C, Chen F. Connections between metabolism and epigenetics in cancers. Semin Cancer Biol 2019;57:52-8.
11. Talukdar S, Emdad L, Gogna R, et al. Metabolic control of cancer progression as novel targets for therapy. Adv Cancer Res 2021;152:103-77.

12. Ghosh P, Vidal C, Dey S, et al. Mitochondria Targeting as an Effective Strategy for Cancer Therapy. Int J Mol Sci 2020;21:3363.
13. Yeung SJ, Pan J, Lee MH. Roles of p53, MYC and HIF-1 in regulating glycolysis - the seventh hallmark of cancer. Cell Mol Life Sci 2008;65:3981-99.
14. Mallo M. Reassessing the Role of Hox Genes during Vertebrate Development and Evolution. Trends Genet 2018;34:209-17.
15. Feng Y, Zhang T, Wang Y, et al. Homeobox Genes in Cancers: From Carcinogenesis to Recent Therapeutic Intervention. Front Oncol 2021;11:770428.
16. Hjalt TA, Murray JC. The human BARX2 gene: genomic structure, chromosomal localization, and single nucleotide polymorphisms. Genomics 1999;62:456-9.
17. Krasner A, Wallace L, Thiagalingam A, et al. Cloning and chromosomal localization of the human BARX2 homeobox protein gene. Gene 2000;250:171-80.
18. Meech R, Makarenkova H, Edelman DB, et al. The homeodomain protein Barx2 promotes myogenic differentiation and is regulated by myogenic regulatory factors. J Biol Chem 2003;278:8269-78.
19. Jones FS, Kioussi C, Copertino DW, et al. Barx2, a new homeobox gene of the Bar class, is expressed in neural and craniofacial structures during development. Proc Natl Acad Sci U S A 1997;94:2632-7.
20. Naka T, Yokose S. Immunohistochemical localization of barx2 in the developing fetal mouse submandibular glands. Acta Histochem Cytochem 2009;42:47-53.
21. Olson LE, Zhang J, Taylor H, et al. Barx2 functions through distinct corepressor classes to regulate hair follicle remodeling. Proc Natl Acad Sci U S A 2005;102:3708-13.
22. Makarenkova HP, Meech R. Barx homeobox family in muscle development and regeneration. Int Rev Cell Mol Biol 2012;297:117-73.
23. Zuo L, Zhu Y, Han J, et al. Circular RNA circSHPRH inhibits the malignant behaviors of bladder cancer by regulating the miR-942/BARX2 pathway. Aging (Albany NY) 2022;14:1891-909.
24. Ma J, Xia LL, Yao XQ, et al. BARX2 expression is downregulated by CpG island hypermethylation and is associated with suppressed cell proliferation and invasion of gastric cancer cells. Oncol Rep 2020;43:1805-18.
25. Lincet H, Icard P. How do glycolytic enzymes favour cancer cell proliferation by nonmetabolic functions? Oncogene 2015;34:3751-9.
26. Zhou L, Li M, Yu X, et al. Repression of Hexokinases II-Mediated Glycolysis Contributes to Piperlongumine-Induced Tumor Suppression in Non-Small Cell Lung Cancer Cells. Int J Biol Sci 2019;15:826-37.
27. Wolf A, Agnihotri S, Micallef J, et al. Hexokinase 2 is a key mediator of aerobic glycolysis and promotes tumor growth in human glioblastoma multiforme. J Exp Med 2011;208:313-26.
28. Katagiri M, Karasawa H, Takagi K, et al. Hexokinase 2 in colorectal cancer: a potent prognostic factor associated with glycolysis, proliferation and migration. Histol Histopathol 2017;32:351-60.
29. Zaret KS, Carroll JS. Pioneer transcription factors: establishing competence for gene expression. Genes Dev 2011;25:2227-41.
30. Li J, Zhang S, Zhu L, et al. Role of transcription factor FOXA1 in non-small cell lung cancer. Mol Med Rep 2018;17:509-21.
31. Wang H, Meyer CA, Fei T, et al. A systematic approach identifies FOXA1 as a key factor in the loss of epithelial traits during the epithelial-to-mesenchymal transition in lung cancer. BMC Genomics 2013;14:680.
32. Luo J, Liu K, Yao Y, et al. DMBX1 promotes tumor proliferation and regulates cell cycle progression via repressing OTX2-mediated transcription of p21 in lung adenocarcinoma cell. Cancer Lett 2019;453:45-56.
33. Tekade RK, Sun X. The Warburg effect and glucose-derived cancer theranostics. Drug Discov Today 2017;22:1637-53.
34. Li L, Liang Y, Kang L, et al. Transcriptional Regulation of the Warburg Effect in Cancer by SIX1. Cancer Cell 2018;33:368-85.e7.
35. DeBerardinis RJ, Lum JJ, Hatzivassiliou G, et al. The biology of cancer: metabolic reprogramming fuels cell growth and proliferation. Cell Metab 2008;7:11-20.
36. Boroughs LK, DeBerardinis RJ. Metabolic pathways promoting cancer cell survival and growth. Nat Cell Biol 2015;17:351-9.
37. Hurley HJ, Dewald H, Rothkopf ZS, et al. Frontline Science: AMPK regulates metabolic reprogramming necessary for interferon production in human plasmacytoid dendritic cells. J Leukoc Biol 2021;109:299-308.
38. Zhang J, Zhang Q. Using Seahorse Machine to Measure OCR and ECAR in Cancer Cells. Methods Mol Biol 2019;1928:353-63.
39. Ngo H, Tortorella SM, Ververis K, et al. The Warburg effect: molecular aspects and therapeutic possibilities. Mol Biol Rep 2015;42:825-34.
40. Ciscato F, Ferrone L, Masgras I, et al. Hexokinase 2 in Cancer: A Prima Donna Playing Multiple Characters. Int J

Mol Sci 2021;22:4716.
41. Castro-Mondragon JA, Riudavets-Puig R, Rauluseviciute I, et al. JASPAR 2022: the 9th release of the open-access database of transcription factor binding profiles. Nucleic Acids Res 2022;50:D165-D173.
42. Zhao M, Tang Z, Wang Y, et al. A direct negative feedback loop of miR-4721/FOXA1/Nanog promotes nasopharyngeal cell stem cell enrichment and metastasis. J Transl Med 2021;19:387.
43. He Y, Wang L, Wei T, et al. FOXA1 overexpression suppresses interferon signaling and immune response in cancer. J Clin Invest 2021;131:e147025.
44. Baca SC, Takeda DY, Seo JH, et al. Reprogramming of the FOXA1 cistrome in treatment-emergent neuroendocrine prostate cancer. Nat Commun 2021;12:1979.
45. Martínez-Reyes I, Chandel NS. Cancer metabolism: looking forward. Nat Rev Cancer 2021;21:669-80.
46. Wang ZH, Peng WB, Zhang P, et al. Lactate in the tumour microenvironment: From immune modulation to therapy. EBioMedicine 2021;73:103627.
47. Chen AN, Luo Y, Yang YH, et al. Lactylation, a Novel Metabolic Reprogramming Code: Current Status and Prospects. Front Immunol 2021;12:688910.
48. Diaz-Moralli S, Tarrado-Castellarnau M, Miranda A, et al. Targeting cell cycle regulation in cancer therapy. Pharmacol Ther 2013;138:255-71.
49. White KA, Grillo-Hill BK, Barber DL. Cancer cell behaviors mediated by dysregulated pH dynamics at a glance. J Cell Sci 2017;130:663-9.
50. Xu Q, Zhang Q, Ishida Y, et al. EGF induces epithelial-mesenchymal transition and cancer stem-like cell properties in human oral cancer cells via promoting Warburg effect. Oncotarget 2017;8:9557-71.
51. Sellar GC, Li L, Watt KP, et al. BARX2 induces cadherin 6 expression and is a functional suppressor of ovarian cancer progression. Cancer Res 2001;61:6977-81.
52. Stevens TA, Meech R. BARX2 and estrogen receptor-alpha (ESR1) coordinately regulate the production of alternatively spliced ESR1 isoforms and control breast cancer cell growth and invasion. Oncogene 2006;25:5426-35.
53. Chen H, Zhang M, Zhang W, et al. Downregulation of BarH-like homeobox 2 promotes cell proliferation, migration and aerobic glycolysis through Wnt/beta-catenin signaling, and predicts a poor prognosis in non-small cell lung carcinoma. Thorac Cancer 2018;9:390-9.
54. Pan C, Li B, Simon MC. Moonlighting functions of metabolic enzymes and metabolites in cancer. Mol Cell 2021;81:3760-74.

(English Language Editor: B. Draper)

Cite this article as: Xie K, Feng J, Fan D, Wang S, Luo J, Ren Z, Zheng C, Diao Y, De Mello RA, Tavolari S, Brandi G, Roden AC, Ren B, Shen Y, Xu L. *BARX2/FOXA1/HK2* axis promotes lung adenocarcinoma progression and energy metabolism reprogramming. Transl Lung Cancer Res 2022;11(7):1405-1419. doi: 10.21037/tlcr-22-465